Influence of heat input and chemical dilution on Critical Pitting Temperature of coatings from Inconel 625 deposited by PTA-P

Raphael A. Lorenzoni[a], Ricardo P. Gasparini[b], Marcelo C. S. Macêdo[c], Eduardo A. Ponzio[d]

Abstract

This study aims at evaluating the influence of heat input and chemical dilution on the Critical Pitting Temperature (CPT) and on the microstructural characteristics of an Inconel 625 weld overlay on an ASTM A36 steel substrate. The coating was made by PTA-P welding. The CPT test was an adaptation of ASTM G150, using a 1.0 mol/L NaCl + 0.025 mol/L $Na_2S_2O_3$ solution. The sodium thiosulfate was determined after exploratory tests. The microstructural characterization was made by chemical analysis by EDX. The results showed that increments of chemical dilution and heat input induced a lower CPT, mainly due to different chemical compositions among the distinct phases. The pitting corrosion resistance was evaluated using a modified PREN, which considers the chemical composition of the dendritic and interdendritic regions separately in which the regions with smaller modified PREN values presented also smaller CPTs. The adopted method proved to be effective for the evaluation of the pitting corrosion resistance of Inconel 625 coatings.

Keywords: Inconel 625, PTA-P, chemical dilution, heat input, CPT.

Introduction

The corrosion of equipment on high temperature and pressure is a problem of several industries, as the petrochemical, thermal, aeronautic and naval. In the case of the oil and gas sector, the petroleum found in reservoirs normally has a high impurity content of corrosive compounds, organic acids, H_2S, CO_2, among others. On this context, the utilization of noble metal coatings over a lowest cost substrate is important.

Research of coating in petroleum extraction and refine are necessary to ensure that the materials quality follows the more severe operation conditions as the faced on pre-salt regions, with higher carbon dioxide, hydrogen sulfide and chlorides content. The combination of these factors can increase corrosion rates severally, and, in case of ineffective control and prediction, can cause severe environmental damage.

Among the materials used as coatings is the UNS N06625, commercially know as Inconel 625, a Ni-Cr-Mo alloy with high mechanical, corrosion and wear resistance. Several processes are utilized to produce the weld overlay, such as MIG/MAG, explosion, TIG and PTA. The latter process is often used due to its high deposition rate and lower heat input (1), achieving

_____
[a,b] Mechanical Engineer – Universidade Federal do Espírito Santo
[c] PhD, Materials Engineer – Universidade Federal do Espírito Santo
[d] PhD, Chemist – Universidade Federal Fluminense

the desired reinforcement on a single pass through feeding metal control. In this study, the influence of heat input and chemical dilution of an Inconel 625 weld overlay made by PTA-P (Plasma Transferred Arc fed with Powder) on its microstructure and pitting corrosion resistance will be evaluated.

Methodology

Plates (220 mm x 100 mm x 12 mm) of carbon structural steel ASTM A36 were used as substrate. The cladding material was Inconel 625 powder, with 53 μm to 150 μm of granulometry, which was deposited using the PTA-P process. The overlay was conducted in a previous work (2). Chemical compositions of both ASTM A36 steel and Inconel 625 powder can be found in Table 1.

Table 1 - Chemical composition (wt. %) of the used materials.

	Chemical composition (wt. %)							
Inconel 625	**Ni**	**C**	**Cr**	**Mo**	**Nb**	**Fe**	**Mn**	**Si**
	64.43	0.01	22.20	9.13	3.53	0.19	0.01	0.05
ASTM A36	**Ni**	**C**	**Cr**	**Al**	**Mn**	**Si**	**Fe**	
	0.02	0.23	0.02	0.03	0.67	0.09	Bal.	

All depositions were made in single-pass, with a 110 mm/min welding speed. The welding position was flat, and the torch was positioned perpendicularly from the steel plate. Pure argon (> 99.9 % purity) was used in the process. A weaving technique was used, with 15 mm width, 1420 mm/min weaving speed, 0.6 Hz weaving frequency and 0.2 s dwell time.

A total of 31 coatings were deposited, using the same welding parameters, except for welding current, powder feed rate, nozzle to workpiece distance (NWD) and recess of the electrode (Rc). The 31 samples were evaluated in previous works (2, 3) in terms of geometrical and chemical dilution, as well as heat input.

In order to evaluate the impact of heat input and chemical dilution in the overall performance of the coatings, two groups of three samples each were created. The first group consisted of coatings with similar heat input and different chemical dilutions (D samples), while the second group had coatings with similar chemical dilution and different heat input (E samples), as seen in Table 2:

Table 2 – Samples characteristics

Sample	Geometric dilution (%)	Chemical dilution (%) - EDX in 1.5 mm of reinforcement	Heat input (J/mm)
D4	3.39	3.76	114
D6	9.22	6.25	117
D12	13.89	11.80	116
E110	5.20	4.94	110
E116	12.35	4.79	116
E133	5.66	4.98	133

Microstructural analysis:

Cross-sections of each clad were ground, polished and then etched with a 92 mL HCl + 5 mL H_2SO_4 + 3 mL HNO_3 solution for 4 min. A Nikon Eclipse MD600 optical microscope was used for initial analysis. Samples were brought to a ZEISS EVO 40 Scanning Electron Microscope (SEM) for further microstructural analysis. The same procedure was used to study the coating surface (with 2 mm of reinforcement). Three area scans on the surface of each coating were made using a SEM with Energy Dispersive X-ray Spectroscopy (EDX) to determine contents of several elements. EDX was also used to determine the elemental composition of several second phases within the sample surface.

Microhardness test:

Three microhardness Vickers profiles were made on the cross-section of each clad using a Pantec HDX – 1000 TM microhardness tester. One of the profiles was made in the middle of the clad, and the others were 3 mm distant from the center. The distance between two measurements within the same profile was 0.2 mm. A 0.1 kg load was applied for 15 s (4).

Electrochemical test:

Corrosion tests consisted of an adaptation of ASTM G150 (5). The solution used was 1 mol/L NaCl + 0.025 mol/L $Na_2S_2O_3$ (6). Table 3 summarizes the adaptations.

A three electrode cell was used: Ag/AgCl as reference electrode, a platinum plate as counter electrode and the working electrode (top surface of the coating). The potential applied during the test was +0.74 V (Ag/AgCl). To prevent crevice corrosion from occurring, a fast drying paint for wood and steel was used. The surface was examined after each test to ensure that no crevice corrosion had occurred.

Table 3 - Summary of the electrochemical test conditions

	ASTM G150	Present study
Solution	1 mol/L NaCl	1 mol/L NaCl + 0.025 mol/L $Na_2S_2O_3$
Test Area	Minimum 1 cm²	Approximately 0.15 cm²
Purging gas	Nitrogen >99.99%	-
Initial test temperature	3 °C	15 °C

Results and discussion

Chemical composition of the coating

The chemical composition of each coating, in 2 mm of reinforcement, is shown in Table 4.

Table 4 - Chemical composition of the coatings by EDX.

Sample	Chemical Composition (wt.%)									
	Ni	Cr	Mo	Nb	Fe	Si	Mn	Al	Ti	Br
D4	62.30	20.37	7.13	4.33	4.23	0.47	0.57	0.47	0.00	0.07
D6	59.83	20.03	7.63	4.30	6.70	0.50	0.47	0.47	0.00	0.00
D12	56.63	19.07	7.20	4.20	11.63	0.47	0.50	0.27	0.00	0.00
E110	61.67	20.27	7.50	4.23	4.90	0.6	0.53	0.23	0.03	0.00
E116	59.63	19.77	7.10	4.40	7.63	0.43	0.57	0.40	0.00	0.00
E133	60.23	20.17	7.47	5.30	5.33	0.47	0.50	0.47	0.00	0.00

As expected, the "D" samples had different iron content, which agrees with the previous works (2, 3). On the other hand, unexpectedly high iron content for the E116 sample was observed. Using the iron contents from Table 4, the new chemical dilutions could be calculated (Table 5):

Table 5 – Chemical dilution of the samples after EDX.

	D4	D6	D12	E110	E116	E133
Geometric dilution (%)	3.39	9.22	13.89	5.20	12.35	5.66
Chemical dilution (%)	4.09	6.60	11.59	4.77	7.54	5.20
Heat input (J/mm)	114	117	116	110	116	133

Microstructure

The microstructures of the cross-sections of all coatings were found to be very similar, consisting mostly of columnar dendrites, growing perpendicularly to the coating-substrate interface. Equiaxial dendrites were also found in the deposits.
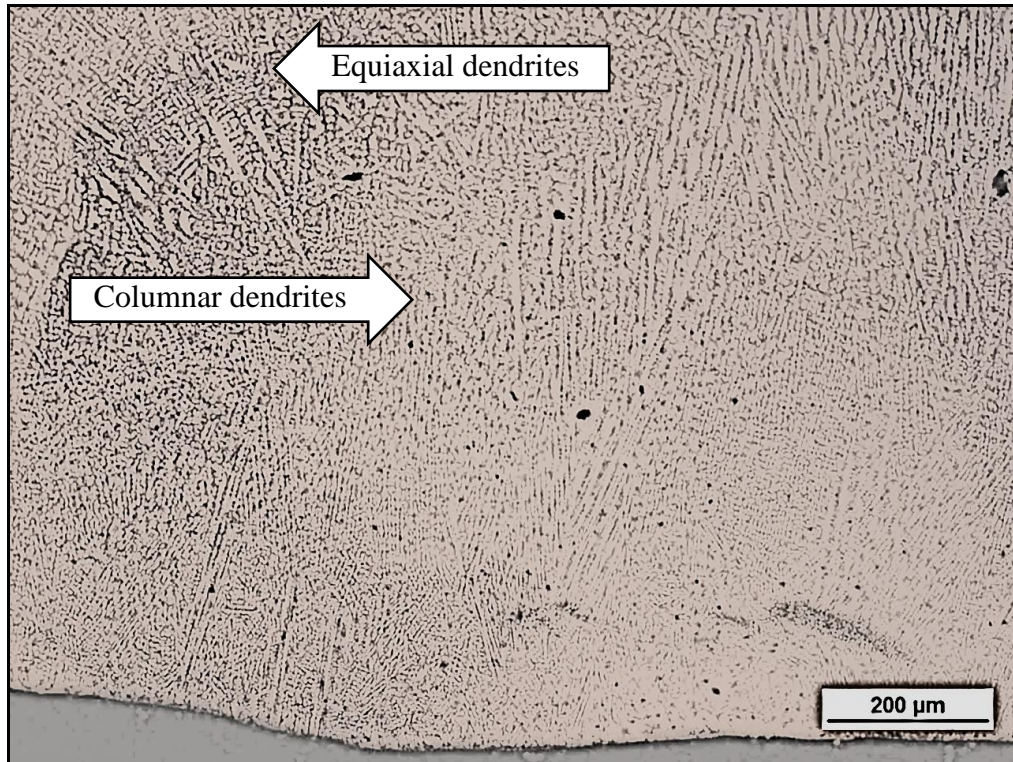
Figure 1 – Optical micrograph of the coating/substrate interface of sample D12 (100x magnification).

ABIOYEA, MCCARTNEY and CLARE (7) showed that the columnar dendrites grow perpendicularly to the interface in Inconel 625 alloys because, during the solidification process, heat is removed from the melting metal mostly by the substrate.

Microhardness test:

For each sample, three microhardness profiles of the cross-sections were obtained. The measurements started 1.6 mm into the substrate and ended 1.4 mm into the clad material. Figure 2 shows the average microhardness values.
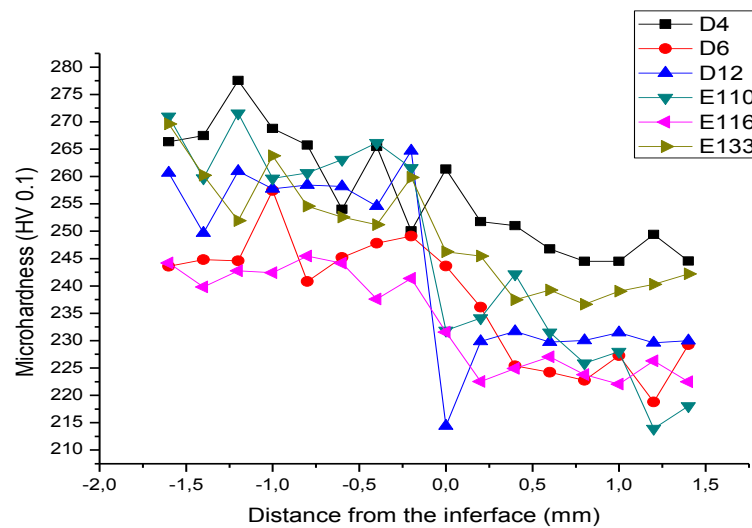
Figure 2 - Microhardness profiles of the coatings.

Low dilution samples presented hardest coatings. According to AGUIAR (8), low dilution implies lower iron content and, therefore, higher contents of elements that are responsible for the hardening mechanisms of Inconel 625, such as molybdenum, niobium and tungsten.

SEM/EDX analysis of the top surface:

Analysis revealed a precipitate-free dendritic region. Second phases were identified in the interdendritic regions. EDX analysis was performed to determine the elemental composition of an average of ten spots per sample, as shown in Figure 3. It is worth noting that due to the small size of the second phases, the measurements can suffer interference from the matrix around and under the spot being analyzed.
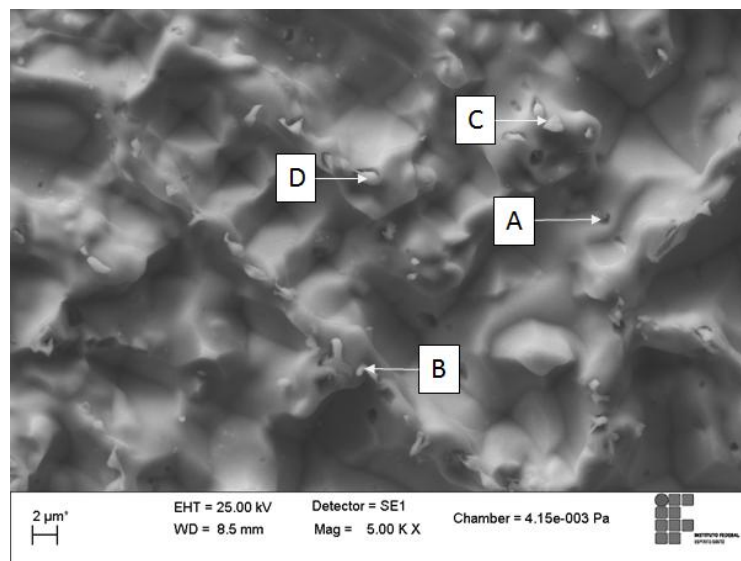

Figure 3 - SEM micrograph of D4 sample. (A), (B), (C) and (D) are second phases that had their elemental composition measured by EDX analysis.

Phases (B) and (C) were considered to be niobium carbides (NbC) due to their high content of niobium and carbon, while phase (A) was identified as Laves phase. High content of boron (60 %) was found in phase (D), which is an indicative of a boride. All other samples presented exclusively NbC and Laves phases.

Using EDX line scan, elemental composition profiles were obtained from the top surface of each sample, as seen in Figure 4.
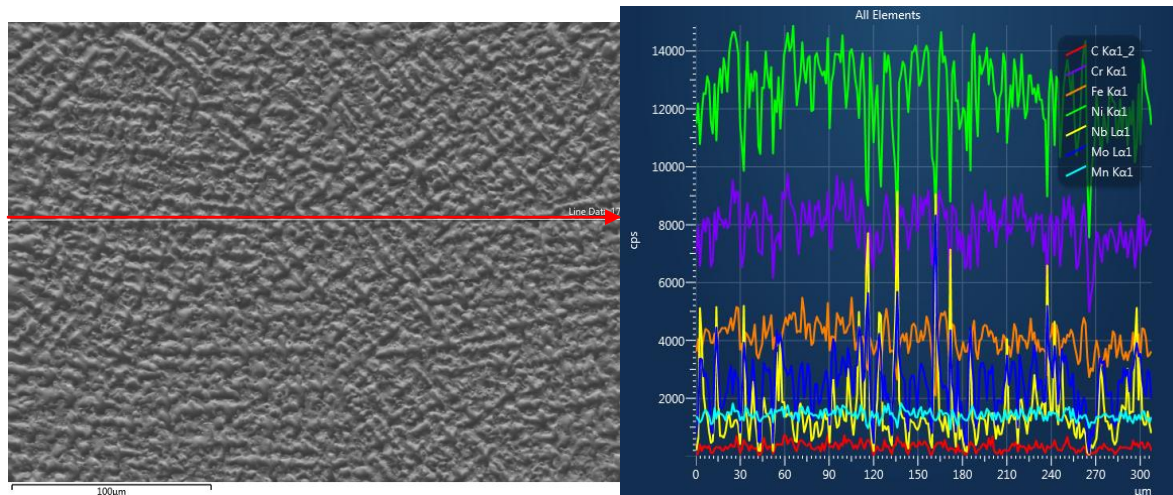

Figure 4 - Elemental composition profile of D12 sample. The micrograph on the left shows the reading direction.

Analyzing the micrograph and the EDX profile simultaneously, it is possible to determine the "Counts Per Second" (CPS) of each element in the dendritic and interdendritic regions separately. It is worth noting that CPS corresponds to the amount of electric pulses that were read by EDX.

In order to obtain a better approximation of the (wt.%) of each element, the CPS was multiplied by the atomic weight and by the energy value of a single pulse for a given element. The result was then divided by sum of the previous for all elements. This approximation for each sample can be seen in Table 6.

Table 6 - Approximate elemental compositions for dendritic and interdendritic regions

Sample	Region	Chemical composition [wt. %]				
		Ni	Cr	Fe	Mo	Nb
D4	Interdendritic	60.3	23.7	5.8	6.5	3.7
	Dendritic	61.6	23.5	5.8	5.7	3.4
D6	Interdendritic	59.2	23.7	8.7	5.8	2.6
	Dendritic	60.0	23.5	9.7	4.9	1.9
D12	Interdendritic	55.9	22.8	15.2	4.2	1.9
	Dendritic	55.4	21.9	14.9	5.1	2.7
E110	Interdendritic	57.4	22.9	6.6	8.3	4.9
	Dendritic	60.6	23.1	7.2	6.3	2.8
E116	Interdendritic	57.9	22.5	10.8	5.8	2.9
	Dendritic	57.6	22.7	11.0	5.9	2.9
E133	Interdendritic	58.8	24.2	7.5	6.1	3.4
	Dendritic	60.6	23.7	7.7	5.7	2.3

These results can be correlated to a study by DUPONT (9), where he analyzes the Equilibrium Distribution Coefficients (k) of Alloy 625 weld overlay deposits. He concluded that Fe, Ni and Cr have a slight tendency to segregate at the dendritic regions, while Mo and especially Nb have a high tendency to segregate at the interdendritic regions.

Exploratory tests

In preliminary tests, the 1.0 mol/L NaCl solution (defined by the ASTM G150 standard), was not sufficient to cause pitting on the samples until the maximum bath temperature (98 °C). TSAI and WU (10) studied the effect of thiosulfate ions and pH in pitting corrosion on an alloy 690 in chloride solutions. They observed a reduction on pitting potential with the increase of thiosulfate concentration until a certain level, and a posterior decrease for higher concentrations. EZUBER (6) analyzed a heat treated Ni-18Cr-6Fe alloy and encountered a 0.025 critical ratio between thiosulfate and chloride ions concentration that generates the maximum reduction of pitting potential.

In order to evaluate if the result found by EZUBER (6) is valid for the alloy 625, exploratory tests were realized with the base solution of 1.0 mol/L NaCl and different concentrations of $Na_2S_2O_3$. The samples in these tests had 12.4 % of geometric dilution and heat input of 141 J/s. The concentrations of sodium thiosulfate were 0.030 mol/L, 0.075 mol/L and 0.150 mol/L. The results of the tests can be seen below:
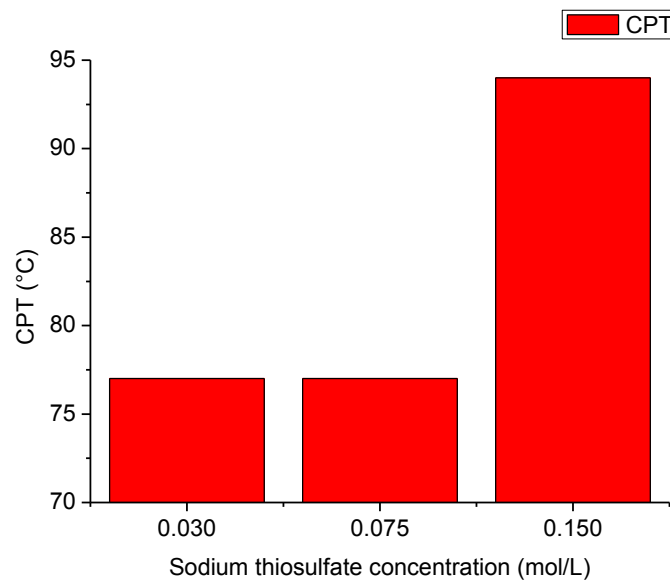
**Figure 5 - CPT results for the exploratory tests in solution of
1.0 mol/L NaCl with different sodium thiosulfate concentrations.**

The solutions of 0.030 mol/L and 0.075 mol/L of $Na_2S_2O_3$ presented the same CPT (77 °C), while the 0.0150 mol/L solution had a CPT of 94 °C, close to the limit temperature of the equipment. To differentiate the two first results, the sample surfaces were analyzed on SEM (Figure 6).
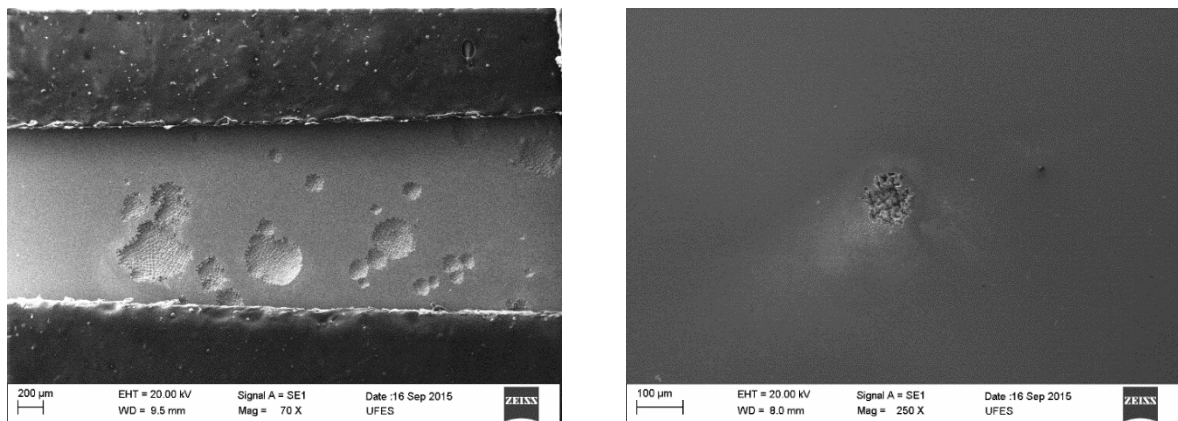

**Figure 6 - SEM images of the sample surfaces after the tests with the base solution and
0.030 mol/L (left) and 0.075 mol/L (right) of $Na_2S_2O_3$.**

It is possible to observe that the thiosulfate concentration of 0.030 mol/L resulted in the formation of a higher quantity of pits, and their dimensions were greater than the single pit encountered on the surface of the sample tested on the concentration of 0.075 mol/L $Na_2S_2O_3$. Thus, the Inconel 625 presented similar results with those reported by EZUBER (6) and the solution utilized for the next tests was 1.0 mol/L NaCl + 0.025 mol/L $Na_2S_2O_3$, considering that this thiosulfate concentration will cause the maximum reduction on pitting potential.

Potentiostatic tests

The results can be seen on Figure 7 and a summary of the tests data on Figure 8. The maximum current density (Imax) was defined as the current density measured 60 s after the same surpasses the limit of 100 μA/cm^2, defined as the limit that corresponds to the pitting formation, accordingly to ASTM G150. This result is presented as an interval of the values observed after each test and not as a standard deviation, due to the stochastic nature of pitting propagation.
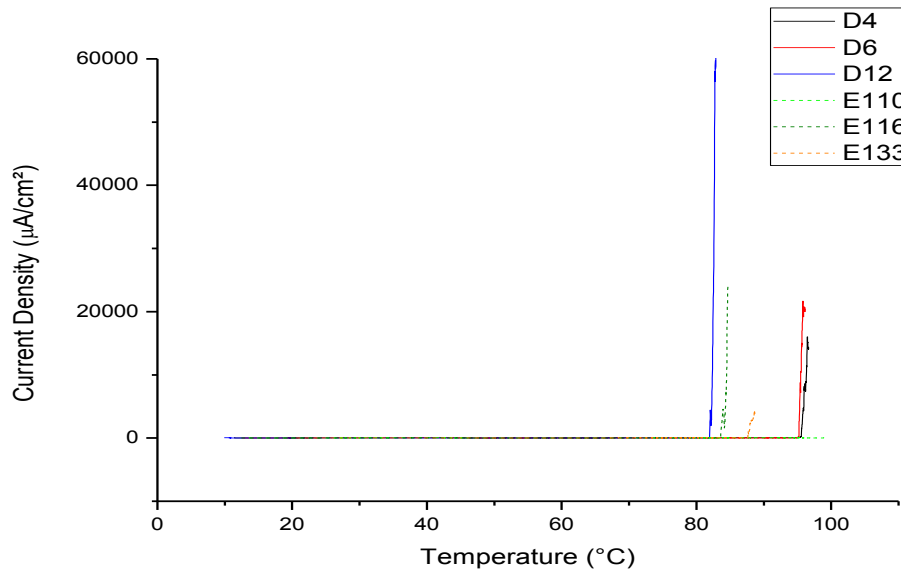

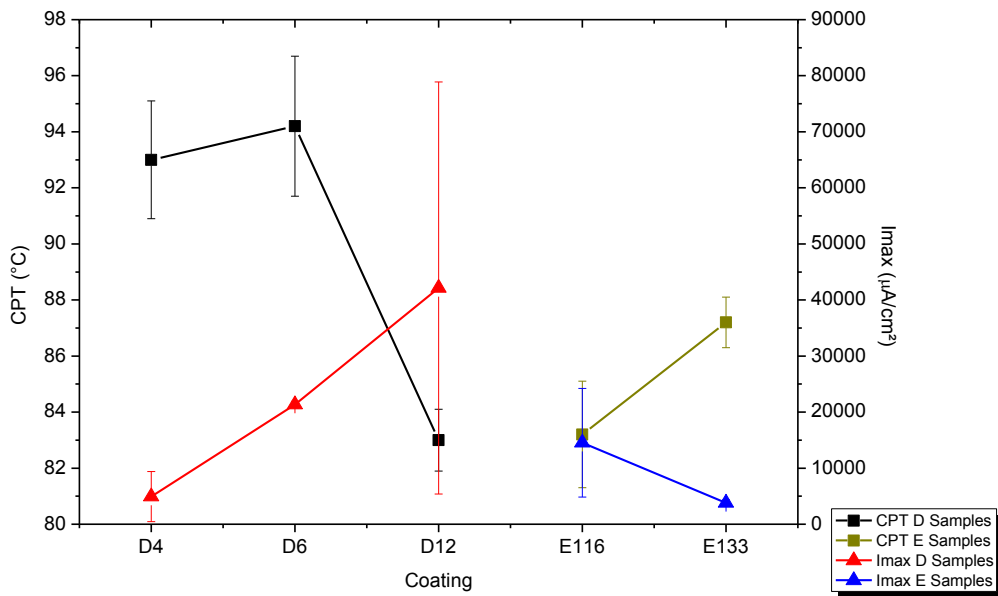**Figure 7 - Graphic representation of CPT results for the coatings.**

Figure 8 - Results summary of the potentiostatic tests.

Coating E110 did not present pitting corrosion during the tests until the temperature of 98 °C. The samples E110 and E133, which have the same chemical dilution but different heat inputs, presented significant difference on their CPT. The higher heat input could have lead the coating to achieve higher temperature peaks during the welding and, consequently, reducing the cooling ratio, enabling the formation of precipitates that have on their structure elements that improve the chloride corrosion resistance, like molybdenum and chromium, reducing the corrosion resistance of the coating.

Among the samples with similar heat inputs (D samples), coatings D4 and D6 presented TCP of 94.2 °C and 93.0 °C, respectively, despite having different chemical dilutions. The coating D12, with chemical dilution of 11.8 %, presented a CPT of 82.7 °C which is significantly lower than the CPT's of D4 and D6. This behavior could be caused by the smaller nickel and chromium content of this sample. It is possible to assume that the chemical dilution and, consequently, the iron content, has a smaller influence as the heat input on pitting corrosion resistance when the iron content is smaller than 6 %. For higher iron content, this effect becomes more significant.

According to CHEN and SZKLARSKA-SMIALOWSKA (11) the presence of borides (found on D4) facilitates pitting initiation and growing, since these regions become active anodic points in the presence of chloride ions.

SIVA and MURUGAN (1) evaluated the effects of PTA-W welding parameters on pitting corrosion resistance of a AISI 316L stainless steel and concluded that the increase in current and, consequently, in heat input, reduces the pitting potential. These conclusions are very similar with the observed for samples E110 and E133. The authors also concluded that the increase in dilution reduces the alloy corrosion resistance.

The higher Imax was observed for sample D12, indicating a higher pitting propagation speed after its initiation, increasing the corrosion rate. The sample D6, despite having a similar CPT to D4, presented a higher Imax. This could have occurred for its higher iron content, that, after the passivation barrier breakage and pitting initiation, enables a faster dissolution of the material due to its associated weak localized corrosion resistance.

Among the E samples, coating E116 presented a higher value of Imax, due to its higher chemical dilution and iron content. The sample E110 does not have an Imax, since it did not present CPT during the tests.

Aiming at evaluating the pitting corrosion susceptibility, the Pitting Resistance Equivalency Number (PREN) is conventionally used in literature as an empiric index that correlates the corrosion-resistant-alloy pitting corrosion resistance with its chemical composition through the following equation:

$$PREN = (wt.\% \; Cr) + 3.3*(wt.\%Mo + 0.5*wt.\%W) + 16*(wt.\%N)$$

For higher PREN values, the higher the pitting corrosion resistance of the material in chlorides. Utilizing the previous chemical composition of the coatings measured by EDS, the following PREN values can be obtained:

Table 7 - PREN estimated by the global chemical composition of the coatings (EDX)

	D4	**D6**	**D12**	**E110**	**E116**	**E133**
PREN	43.9	45.2	42.8	45.0	43.2	44.8

The PREN of the powder utilized as filler metal is 53.2. Observing the previous table, the global chemical analysis of the coatings satisfies the results found in this work for both families. However, the sample D6 presented a PREN higher than E110, which does not correspond to the results. In order to find a better correlation, initially, the sample surfaces were analyzed using optical microscopic.
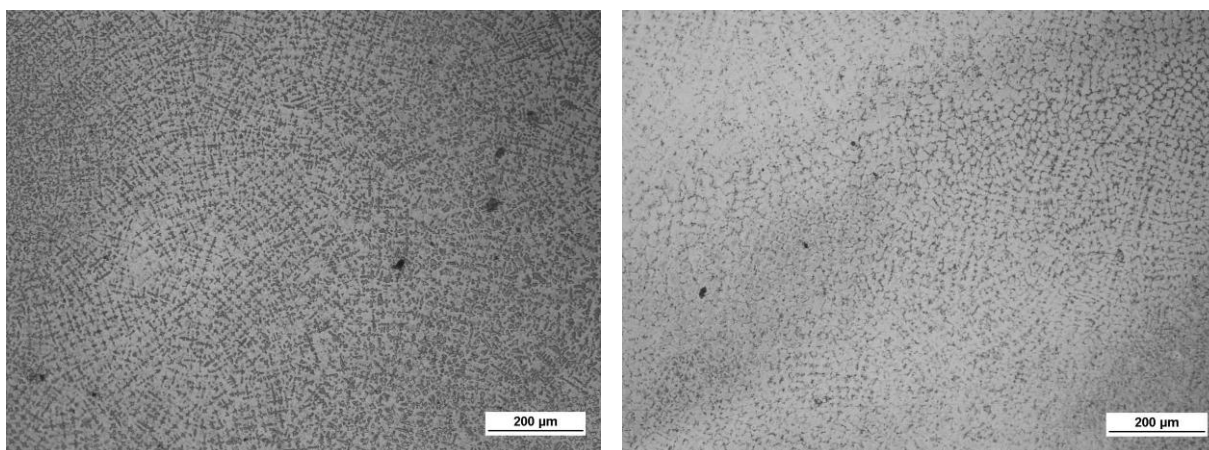

Figure 9 - Surfaces of E110 (left) and E116 (right) samples after the potentiostatic tests by optical microscopy (100x magnification).

The samples D12 and E116 presented preferential attack in interdendritic regions, while the samples E110, E133 and D4 presented preferential attack in dendritic regions. The sample D6 presented attacked zones in both regions simultaneously, dendritic and interdendritic. It is possible to use the results from Table 6 to evaluate the PREN of these regions separately. The results are shown in Figure 10.
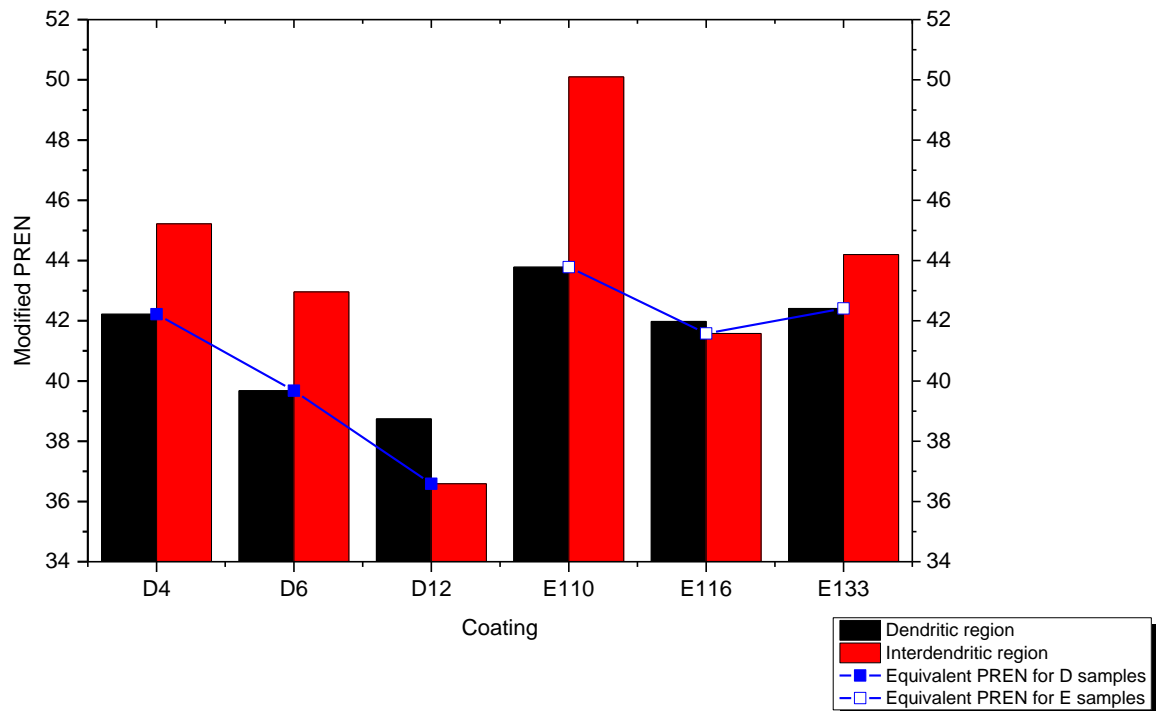
Figure 10 - Modified PREN for the specific regions of the coatings.

For the samples E110, E133, D6 e D4, the modified PREN of the interdendritic regions were higher than its values for the dendritic regions, while the coatings E116 and D12 presented the inverse behavior, corroborating with the results found before.

The sample D6 presented, on the micrographs, well distinguished regions of interdendritic and dendritic corrosion. This occurrence could be assigned to the different temperature profiles developed during the welding and the different cooling rates, allowing some regions to benefit the formation of precipitates, which contains elements that increases the corrosion resistance of the matrix, in special the molybdenum. The precipitation reduces the content of this element on the interdendritic region and favors the local pit nucleation.

The utilization of the modified PREN showed itself more concise with the results found in the potentiostatic tests than the PREN with the coatings global chemical composition. The samples E116 e D12 presented the smaller modified PRENs, while E110 presented the highest value. PESSOA (12), when investigating the CPT of Inconel 625 and Hastelloy C-276 alloys deposited by MIG/MAG welding through immersion tests in acidified iron chloride solutions, concluded that the smaller heat input increased the CPT due to the higher iron content on the coating, presenting similar results with this work.
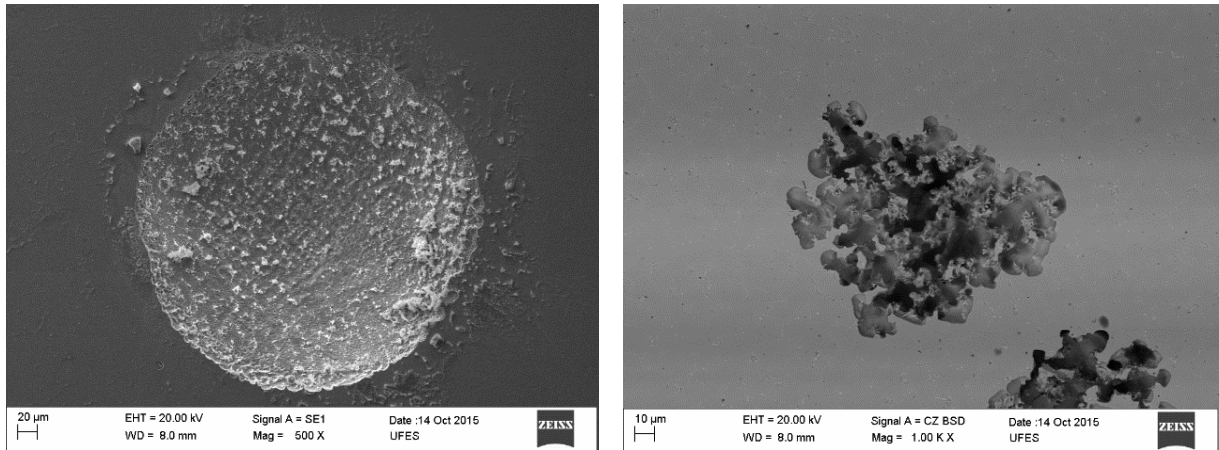
Figure 11: Pits on the surface of samples D6 and D12 after the electrochemical tests by SEM.

From Figure 11, the samples E116 and D6 presented pits with great dimensions in circular format, that corroborates with the higher values of Imax from the potentiostatic tests, which indicates a higher corrosion intensity. In the revision made by FRANKEL (13), he mentions that molybdenum was not found in the protective layers of stainless steels, although was present on the surface of active sites, blocking the dissolution on these areas. Samples E116 and D6 presented molybdenum contents slightly lower, which can explain the results encountered.

On samples D12 and D4, it is possible to observe that the pit propagation occurred preferentially at the dendritic regions with no corrosion at interdendritic regions. The D12 coating presented pits with smaller dimensions, however, in greater quantity on the surface, explaining the higher values of Imax in the tests. D4 presented pits with great dimensions in some tests and small dimensions in others, justifying the great variation in Imax.

Sample E133 presented pits, preferably, on a single dendrite, which indicate a low pit propagation speed, where the corrosion site remained on a single region.

Based on the results above, it is possible to conclude that the adaptation of ASTM G150 (5) standard with the addition of 0.025 mol/L $Na_2S_2O_3$ was effective for the evaluation of pitting corrosion resistance of Inconel 625 coatings made by a single pass with PTA-P welding, extending the results found by EZUBER (6). The sodium thiosulfate reduced the CPT for the Inconel 625 which was not possible to evaluate only with a sodium chloride solution. The increase in chemical dilution and heat inputs decreases the pitting corrosion resistance, preferably in the regions that have a smaller content of molybdenum, due to segregation during the solidification process.

Conclusions

- The microhardness of the coatings on samples with lower chemical dilution presented higher values;
- The microstructure presented a γ matrix with the presence of precipitates in interdendritic regions;
- The precipitates are, mainly, Laves phase and NbC, and in sample D4, borides were also detected;

- • The lower heat input benefits a higher CPT, indicating a higher pitting corrosion resistance. The chemical dilution increase lowers the CPT and that reduction is more significant for chemical dilution values higher than 6 %;
- • The higher iron content induces greater current after the protective barrier breakage and, consequently, pitting initiation due to its lower oxidation resistance, causing pitting growing, which can be proved by the presence of pits with greater dimensions;
- • Corrosion occurs preferentially in regions with smaller PREN, i.e., with lower molybdenum and chromium content;
- • The CPT evaluation through the modified PREN for dendritic and interdendritic regions proved more adequate than the PREN evaluation with the global chemical composition of the sample. A trend was observed, where the smaller PREN values between these regions determined the coating's CPT;
- • The CPT methodology utilized on this work proved to be adequate to evaluate the coating pitting corrosion resistance.

Acknowledgements

References

(1) SIVA, K.; MURUGAN, N. A Study on the Influence of PTAW Process Parameters on Pitting Corrosion Resistance of Nickel Based Overlays. **Procedia Engineering**, v. 64, p. 1147-1156, 2013.

(2) SILVA, L. C. C.; CANAL, A.; LUZ, T. S. **Estudo de parâmetros e processos em aço carbono revestidos com Inconel 625 utilizando o Processo PTA-P.** 7° Congresso Brasileiro de P&D em Petróleo e Gás. Aracaju, 2013.

(3) VIDAL, F. A. **Análise composicional em revestimento de Inconel 625 depositados por PTA-P em aço ASTM A36**. Final project (Bachelor in Mechanical Engineering) - Universidade Federal do Espírito Santo, Vitória, 2014.

(4) ASTM INTERNATIONAL**. ASTM E384 - Standard Test Method for Microindendation Hardness of Materials**. West Conshohocken, 1999.

(5) ASTM INTERNATIONAL. **ASTM G150 - Standard Test Method for Electrochemical Critical Pitting Temperature Testing of Stainless Steels**. West Conshohocken, 1999.

(6) EZUBER, H. M. Role of Thiosulfate on Chloride Breakdown Potential of Heat Treated Ni-18Cr-6Fe Alloys. **Journal of ASTM International**, West Conshohocken, v. 6, n. 3, June 2009.

(7) ABIOYE, T. E.; MCCARTNEY, D. G.; CLARE, A. T. Laser cladding of Inconel 625 wire for corrosion protection. **Journal of Materials Processing Technology**, Nottingham, n. 217, p. 232-240, 2015.

(8) AGUIAR, W. M. **Revestimento por soldagem MIG/MAG empregando ligas de níquel para aplicações em componentes do setor de petróleo e gás natural**. Thesis (Doctor in Materials Science and Engineering) - Universidade Federal do Ceará. Fortaleza, 2010.

(9) DUPONT, J. N. Solidification of an Alloy 625 Weld Overlay. **Metallurgical and Materials Transactions A**, 27A, 1996. 3612-3620.

(10) TSAI, W. T.; WU, T. F. Pitting Corrosion of Alloy 690 in thiosulfate-containing chloride solutions. **Journal of Nuclear Materials**, n. 277, p. 169-174, 2000.

(11) CHEN, T. Y.; SZKLARSKA-SMIALOWSKA, Z. The pitting corrosion characteristics of boride-strengthened nickel- and iron-based microcrystalline alloys. **Corrosion Science**, v. 28, n. 1, p. 97-107, 1988.

(12) PESSOA, E. F. **Soldagem de revestimento com ligas de níquel empregando o processo MIG/MAG com duplo arame para aplicações em componentes do setor de petróleo e gás natural**. Thesis (Doctor in Materials Science and Engineering) - Universidade Federal do Ceará, Fortaleza, 2014

(13) FRANKEL, G. S. Pitting Corrosion of Metals A Review of the Critical Factors. **Journal of the Electrochemical Society**, v. 145, n. 6, p. 2186-2198, 1998.